AFRL-RH-FS-TR-2023-0002

Probabilistic Water Bidirectional Reflectance Distribution Function, Version 2

Albert W. Bailey
Edward A. Early
Elharith Ahmed
SAIC

Andrew W. Wharmby
Semih S. Kumru
711th Human Performance Wing
Airman Systems Directorate
Bioeffects Division
Optical Radiation Branch

08 January 2023

January 2019 – January 2023

Air Force Research Laboratory
711th Human Performance Wing
Airman Systems Directorate
Bioeffects Division
Optical Radiation Bioeffects Branch
JBSA Fort Sam Houston, Texas 78234

NOTICE AND SIGNATURE PAGE

"Probabilistic Water Bidirectional Reflectance Distribution Function, Version 2"

(AFRL-RH-FS-TR- 2023- 0002) has been reviewed and is approved for publication in accordance with assigned distribution statement.

FERRIS.LYNDSEY.
MARIE.1381070391

Digitally signed by
FERRIS.LYNDSEY.MARIE.1381070391
Date: 2023.01.24 08:53:13 -06'00'

LYNDSEY M. FERRIS, LtCol, USAF, BSC
Chief, Optical Radiation Bioeffects Branch

MILLER.STEPHANI
E.A.1230536283

Digitally signed by
MILLER.STEPHANIE.A.1230536283
Date: 2023.03.21 11:56:14 -05'00'

STEPHANIE A. MILLER, DR-IV, DAF
Chief, Bioeffects Division
Airman Systems Directorate
711th Human Performance Wing
Air Force Research Laboratory

REPORT DOCUMENTATION PAGE

Form Approved
OMB No. 0704-0188

1. REPORT DATE *(DD-MM-YYYY)*	2. REPORT TYPE	3. DATES COVERED *(From - To)*
08-01-2023	Interim Technical Report	Jan 2019 – Jan 2023

4. TITLE AND SUBTITLE
Probabilistic Water Bidirectional Reflectance Distribution Function, Version 2

5a. CONTRACT NUMBER
FA8650-19-C-6024

5b. GRANT NUMBER

5c. PROGRAM ELEMENT NUMBER

6. AUTHOR(S)
Albert Bailey, Edward Early, Elharith Ahmed, Andrew Wharmby, Semih Kumru

5d. PROJECT NUMBER

5e. TASK NUMBER

5f. WORK UNIT NUMBER
H14B

7. PERFORMING ORGANIZATION NAME(S) AND ADDRESS(ES)
Air Force Research Laboratory
711th Human Performance Wing
Airman Systems Directorate
Bioeffects Division
Optical Radiation Bioeffects
JBSA, Fort Sam Houston, Texas 78234

4141 Petroleum Rd
Fort Sam Houston, Texas 78234

8. PERFORMING ORGANIZATION REPORT

9. SPONSORING / MONITORING AGENCY NAME(S) AND ADDRESS(ES)
711th Human Performance Wing
Airman Systems Directorate
Bioeffects Division
Optical Radiation Branch
JBSA, Fort Sam Houston, Texas 78234

10. SPONSOR/MONITOR'S ACRONYM(S)
711 HPW/RHDO

11. SPONSOR/MONITOR'S REPORT NUMBER(S)
AFRL-RH-FS-TR-2023-0002

12. DISTRIBUTION / AVAILABILITY STATEMENT
Distribution A. Approved for public release; distribution is unlimited. CLEARED: PA CASE # AFRL-2023-1384. The opinion expressed on this document, electronic or otherwise, are solely those of the authors. They do not represent an endorsement by or the views of the United States Air Force, the Department of Defense, or the United States Government.

13. SUPPLEMENTARY NOTES

14. ABSTRACT
Reflections of a laser beam from a water surface are inherently probabilistic, depending on the surface state at the particular location and time. Measured statistics on wave states allow probabilistic calculations of wave height and slope at the location and time of reflections. These, in turn, are used to calculate the bidirectional reflectance distribution function (BRDF) in a probabilistic sense based on multiple deterministic BRDF values. A complete model of probabilistic water BRDF is detailed, with accompanying illustrations of BRDF for selected conditions. In general, the BRDF decreases rapidly with increasing wind speed, and the probabilistic BRDF is significantly less than the deterministic BRDF under identical conditions. An empirical model of water BRDF for more rapid calculations is based on results from the probabilistic model.

15. SUBJECT TERMS
BRDF, Probabilistic BRDF, Water reflections, Laser hazards

16. SECURITY CLASSIFICATION OF: Unclassified			17. LIMITATION OF ABSTRACT	18. NUMBER OF PAGES	19a. NAME OF RESPONSIBLE PERSON
a. REPORT	b. ABSTRACT	c. THIS PAGE			Andrew Wharmby
U	U	U	SAR	33	19b. TELEPHONE NUMBER *(include area code)* 210-539-8284

Standard Form 298 (Rev. 8-98)
Prescribed by ANSI Std. 239.18

This Page Intentionally Left Blank

TABLE OF CONTENTS

LIST OF FIGURES

LIST OF TABLES

1.0 INTRODUCTION

Water is a reflecting surface, and therefore can be a hazard source when illuminated by a laser beam. Personal experience of sunlight reflected from bodies of water, usually described in terms of glint, illustrates the dynamic nature of reflections and the role of the structure of the surface [1]. A smooth surface has a nearly constant glint pattern, while the glint pattern becomes more variable as the surface becomes less smooth. The roughness of the water surface increases monotonically as the wind speed increases, so lower wind speeds imply smoother surfaces. The bidirectional reflectance distribution function (BRDF) quantifies the reflecting properties of a surface. The surface of water has reflecting features over many length scales, from small ripples to large swells. These features depend on the wind speed, with windier conditions generally leading to a rougher surface. Waves are the primary feature of a water surface, and their variability obviously complicates a BRDF model. While not completely stochastic, waves do have variability over location and time, and models exist to quantify the features of waves [2]. A combination of models, one for small-scale features and another for large-scale, provides the basis for a probabilistic BRDF of a water surface.

The significant changes from the previous version of this technical report [3] are: removal of water temperature as an input, calculation of the minimum wave number based on the wind friction velocity, refinement of the reflected beam obscuration calculation, revision of the smooth water BRDF, replacing the normalization factor with a shadowing function and revising the normal variances, revision of examples, and addition of an empirical water BRDF model.

2.0 OVERVIEW OF MODEL

The probabilistic water BRDF model has two main components – smooth water BRDF and wave motion. The first applies to length scales smaller than the laser beam diameter, where the BRDF is deterministic and based on water slope variances [4]. These variances depend on the wind speed and the beam diameter. The second component applies to longer length scales and is based on the wave energy spectrum, resulting in a probabilistic BRDF [5]. The wave energy spectrum depends on the wind speed and direction and is comprised of sine waves with different wave numbers and phases. A set of wave numbers and phases determines the surface height as a function of location and time. Each such set is an instance for the spectrum, and a set of instances provides the probabilistic aspect of the model. The location and direction of the laser beam at a given time provide an intersection location on and normal to the water surface for each instance. When combined with an observer location, these determine the geometry of the reflection and a BRDF based on the water slope variances. Accumulation of the BRDFs over all instances provides the statistics of the BRDF. All locations and times in a simulation use the same instances of the wave energy spectrum.

The process of calculating a probabilistic water BRDF is illustrated in Fig. 1. The locations of the laser and an observer, and the direction of the laser beam, describe a laser engagement scenario. These quantities may change over the course of the scenario. Other required quantities, such as the wind speed, are taken to be constant over the scenario. The nature of these input parameters is indicated as either static or dynamic in Fig. 1. The wave energy spectra depend upon the wind speed and wave number. For a given scenario, a number N of instances of the wave spectra are generated from a finite number M of random wave numbers, angles, and phases, with each instance using a different set of wave numbers, angles, and phases. For each instance, the laser beam intersects the surface of the water, and a BRDF in the direction of the observer is calculated. The statistics of the BRDF are determined from the multiple instances.

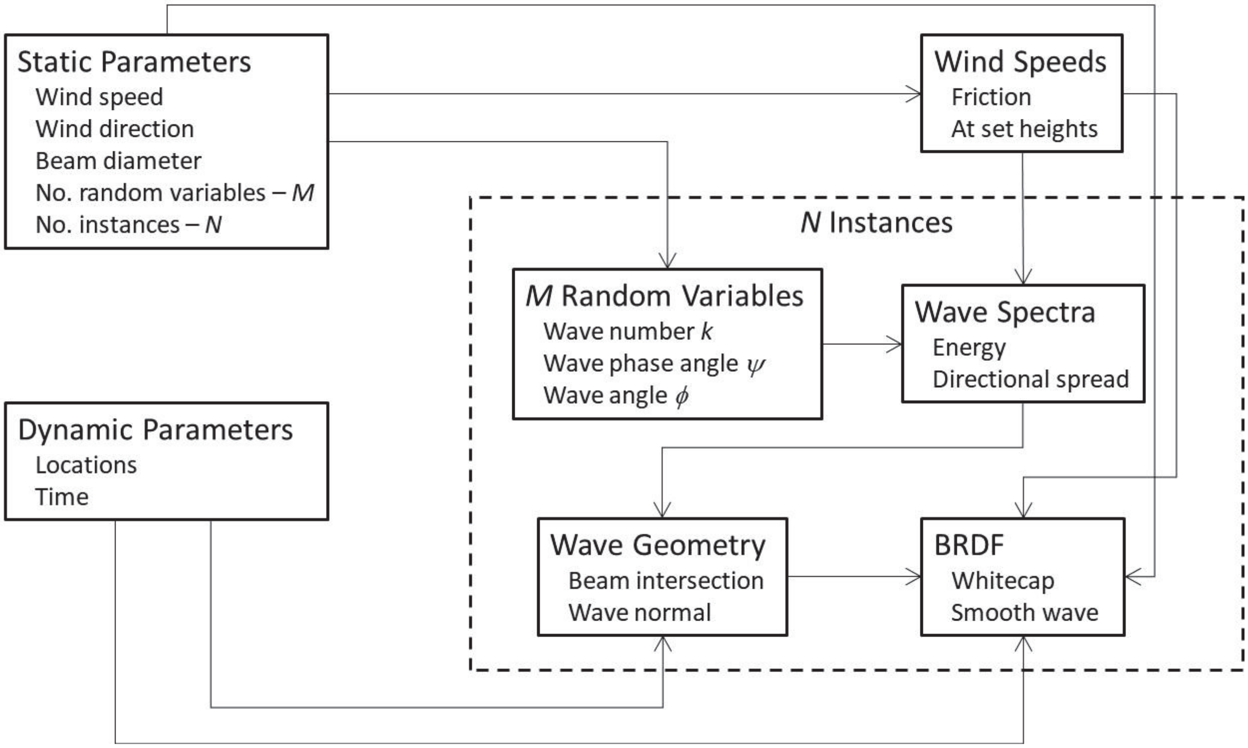

Figure 1. Elements of the probabilistic water BRDF model

The probabilistic water BRDF model uses both meter-kilogram-second (mks) and centimeter-gram-second (cgs) units, as appropriate for the calculation. The default unit is mks, but the natural unit for the wind friction velocity is cgs, so wind speeds and wave energy spectra are expressed in this unit.

3.0 WIND SPEEDS

Wind speed determines wave energy spectra, and wind speeds at different heights are required in various calculations. These speeds are denoted by W_h, where W is the speed and h is the height above the mean water surface. The wind speed at any height [6] is

$$W(h) = W_h = \frac{w^*}{\kappa} \ln\left(\frac{h}{h_0}\right) , \tag{1}$$

where w^* is the wind friction velocity, and the roughness height h_0 is

$$h_0(w^*) = \frac{0.684}{w^*} + 4.28 \times 10^{-5} (w^*)^2 - 0.0443 . \tag{2}$$

The von Kármán constant $\kappa = 0.4$, and cgs units apply to both equations. Given a wind speed and height, Eqs. (1) and (2) are solved iteratively to yield a wind friction velocity. Once the wind friction velocity is known, the wind speed at any height is given by Eq. (1). Wind speeds used in subsequent calculations are those at heights of 10 m, 12.5 m, and 19.5 m, denoted by W_{10}, $W_{12.5}$, and $W_{19.5}$, respectively.

The Beaufort Scale is a common method for assigning wind speeds to water surface conditions [7]. The Beaufort number and corresponding wind speed and wave friction velocities are given in Table 1. Lasers are not expected to be operated in conditions worse than a strong breeze, so only Beaufort Numbers from 0 to 6 are used when calculating results from the probabilistic water BRDF model. The corresponding wind friction velocities used in subsequent calculations are 2, 4, 8, 16, 24, 40, and 56 cm/s, respectively.

Table 1. Beaufort numbers and corresponding wind speeds

Beaufort Number	Description	W_{10} (m/s)		w^* (cm/s)	
		Range	Nominal	Range	Nominal
0	Calm	0 – 0.5	0.25	0 – 2.40	1.31
1	Light air	0.5 – 1.5	1.0	2.40 – 6.24	4.40
2	Light breeze	2 – 3	2.5	7.98 – 11.20	9.62
3	Gentle breeze	4 – 5	4.5	14.18 – 17.08	15.62
4	Moderate breeze	6 – 8	7.0	20.23 – 28.80	24.08
5	Fresh breeze	9 – 11	10.0	34.02 – 45.10	39.47
6	Strong breeze	11 – 14	12.5	45.10 – 62.90	53.83
7	Near gale	14 – 17	15.5	62.90 – 82.08	72.31
8	Gale	17 – 21	19.0	82.08 – 109.88	95.66
9	Severe gale	21 – 24	22.5	109.88 – 132.45	120.98
10	Storm	25 – 28	26.5	140.31 – 164.93	152.42
11	Violent storm	29 – 32	30.5	173.49 – 200.26	186.67
12	Hurricane	33 – 36	34.5	209.57 – 238.65	223.89

4.0 WAVE ENERGY SPECTRA

The height and normal of the water surface vary with location and time, and variations of these are important for the BRDF of water as time advances and locations change during a simulation. Waves on the sea are decomposed into a superposition of sine waves of different wavelengths, amplitudes, and directions.

The wave energy depends on the wave number and wind speed. The wave number k (rad/cm) is

$$k = \frac{2\pi}{\lambda}, \tag{3}$$

where λ is the wavelength of the wave. The dispersion relation is

$$\omega^2 = \left(gk + \frac{\tau k^3}{\rho}\right)\tanh(kd)\,, \tag{4}$$

where ω (rad/s) is the angular frequency, g is the acceleration of gravity, τ is the water surface tension, ρ is the water density, and d (cm) is the water depth [5]. Values for these quantities are g = 981 cm/s^2, τ = 76.3 dyne/cm, and ρ = 1.0 g/cm^3 for fresh water and 1.025 g/cm^3 for oceanic salt water. Surface tension effects are negligible for wavelengths longer than a meter, while the hyperbolic tangent term goes to unity for deep water.

There are a variety of wave spectra models, the best ones being combinations of fits for different wavelength ranges. Aguirre et al. use the Bjerkaas-Reidel wave spectrum [8] with five wavelength ranges. Wavelengths shorter than the laser diameter at the water surface are unimportant when determining the water normal, although they are important for the deterministic BRDF.

Constants used in the calculation of wave energy are $\alpha = 8.1 \times 10^{-3}$, $\beta = 0.74$, k_2 from Eq. (4) for which $\omega = 20\pi$ rad/s (for large d, $k_2 = 2.647$ rad/cm for fresh water and 2.659 rad/cm for salt water),

$$k_m = \sqrt{\frac{g\rho}{\tau}}\,, \tag{5}$$

$$p = 5 - \log_{10}(w^*)\,, \tag{6}$$

$$k_0 = \sqrt{\frac{2\beta}{3}\frac{g}{W_{19.5}^2}}\,\text{, and} \tag{7}$$

$$k_1 = \left(\frac{\alpha}{0.875}\right)^2\left(\frac{g}{4\pi^2}\right)^{p-1}\left[k_2\left(1+\frac{k_2^2}{k_m^2}\right)\right]^{p-4}\frac{\left(1+\frac{k_1^2}{k_m^2}\right)^5}{\left(1+\frac{3k_1^2}{k_m^2}\right)^2}\,, \tag{8}$$

where Eq. (8) is solved iteratively.

For a given wave number k, the wave energy spectra $S(k)$ is given by the following procedure. In the Pierson-Moskowitz range, for which $k \le k_0$,

$$B = \frac{\beta g^2}{W_{19.5}^4} = \frac{3}{2}k_0^2 \text{ and} \tag{9}$$

$$S(k) = S_1(k) = \frac{\alpha}{2k^3}\exp\left(-B/_{k^2}\right)\,. \tag{10}$$

If the location of the engagement is less than 100 km from the shore, the effect of wave fetch can be significant if the wind is blowing away from land [9]. The correction for wave fetch applies a multiplicative correction to Eq. (10) of 3.3^r, where

$$r = \exp\left[-\frac{\left(\omega(k) - \omega_p\right)^2}{s \cdot \omega_p^2}\right], \tag{11}$$

$$\omega_p = 22\left(\frac{g^2}{X \cdot W_{10}}\right)^{1/3}, \tag{12}$$

$$s = \begin{cases} 0.0098 & \text{for } \omega \le \omega_p \\ 0.0162 & \text{for } \omega > \omega_p \end{cases}, \tag{13}$$

and X is the distance to the shore in the direction from which the waves originate.

In the Stacey range, for which $k_0 < k \le k_1$,

$$S_{St}(k) = (271.5 + 13.585\, w^*)\sqrt{\frac{g}{k}}\exp\left[2.53\left(0.4\pi - \sqrt{gk}\right)\right] \text{ and} \tag{14}$$

$$S(k) = \begin{cases} \max[S_1(k), S_{St}(k)] & \text{for } w^* \ge 35.8 \text{ cm/s} \\ S_1(k) & \text{for } w^* < 35.8 \text{ cm/s} \end{cases}. \tag{15}$$

Finally, in the Kitaigorodskii range, for which $k_1 < k \le k_2$,

$$S_2(k) = 0.4375\left(\frac{2\pi}{\sqrt{g}}\right)^{p-1} \frac{1 + 3\dfrac{k^2}{k_m^2}}{\left[k_2\left(1 + \dfrac{k_2^2}{k_m^2}\right)\right]^{\frac{p-4}{2}}\left[k\left(1 + \dfrac{k^2}{k_m^2}\right)\right]^{\frac{5}{2}}} \tag{16}$$

and

$$S(k) = \begin{cases} \max[S_{St}(k), S_2(k)] & \text{for } w^* \ge 75.76 \text{ cm/s} \\ S_2(k) & \text{for } w^* < 75.76 \text{ cm/s} \end{cases}. \tag{17}$$

The expressions for $S(k)$ are one-dimensional wave energy spectra. The full wave spectrum [2], including direction and phase, is

$$S(k, \phi) = S(k)\, F(k, \phi), \tag{18}$$

where the directional spreading function F is

$$F(k, \phi) = F(\phi) = \begin{cases} \dfrac{2(1-A)}{\pi}\cos^2(\phi - \phi_W) + \dfrac{A}{\pi} & \text{for } -\dfrac{\pi}{2} < (\phi - \phi_W) < \dfrac{\pi}{2}, \\ 0 & \text{otherwise} \end{cases} \tag{19}$$

where $A = 0.2$, ϕ_W is the wind direction, and

$$\int_{-\pi}^{\pi} F(\phi)\, d\phi = \int_{-\pi/2}^{\pi/2} F(\phi) d\phi = 1 \ . \tag{20}$$

The wave energy spectrum for selected values of wind friction velocity are shown in Fig. 2.

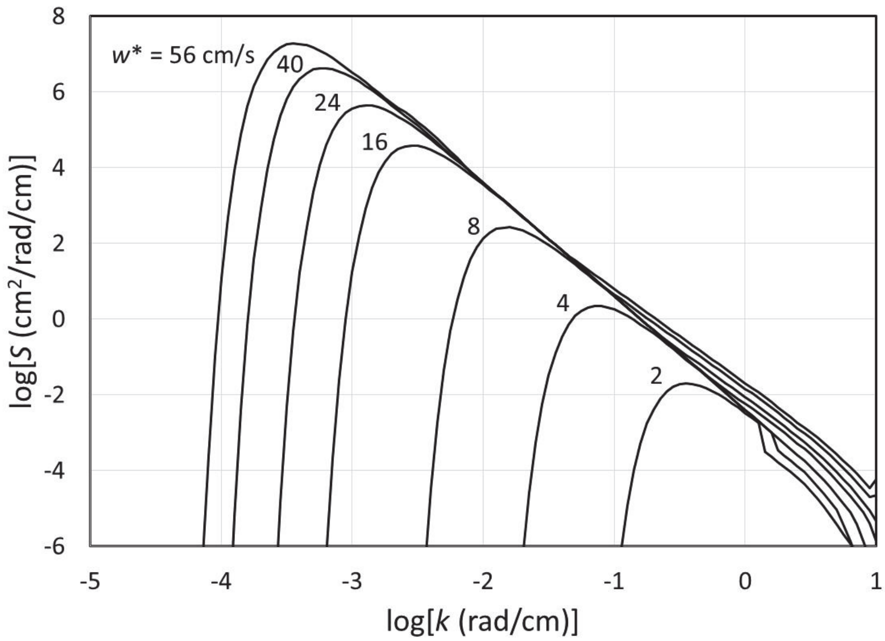

Figure 2. Wave energy spectra for indicated values of wind friction velocity *w**

The instances of wave energy spectra are indexed by $i = 1$ to N, with each instance composed of $j = 1$ to M random wave numbers k_j, wave phase angles ψ_j, and wave angles ϕ_j. Wave numbers are limited to the range

$$\log(k_{\mathrm{min}}) = -2.108 \log(w^*) - 0.267 \quad \text{and} \tag{21}$$

$$k_{\mathrm{max}} = \max\left[k_2, \max\left(\frac{2\pi}{f\,D}, \sqrt{10}\, k_{\mathrm{min}}\right)\right] \ , \tag{22}$$

where D (cm) is the beam diameter and typically $f = 2$. Random wave numbers are drawn from the uniform distribution

$$\tilde{k}_j \in [\ln(k_{\mathrm{min}}), \ln(k_{\mathrm{max}})] \tag{23}$$

with

$$k_j = \exp(\tilde{k}_j) \ . \tag{24}$$

The extent L of the wave numbers is

$$L = [\ln(k_{\mathrm{max}}) - \ln(k_{\mathrm{min}})] \ . \tag{25}$$

Random wave phase angles are drawn from the uniform distribution

$$\psi_j \in [0, 2\pi] \tag{26}$$

and random wave angles are drawn from the uniform distribution

$$\phi_j \in \left[\phi_W - \frac{\pi}{2}, \phi_W + \frac{\pi}{2}\right] . \tag{27}$$

5.0 WAVE GEOMETRY

The wave geometry for each instance $i = 1$ to N determines the location of intersection of the laser beam with the surface of the water, and the normal of the water surface at that location. The wave geometry depends on the location (x, y) and time t. At each time t, the laser and observer are at locations $\vec{r}_L$ and $\vec{r}_O$, respectively. The direction $\hat{k}_L$ of the laser beam is given or calculated from a target location $\vec{r}_T$ with

$$\hat{k}_L = \frac{\vec{r}_T - \vec{r}_L}{\|\vec{r}_T - \vec{r}_L\|} . \tag{28}$$

A location $\vec{r}$ along the laser beam is therefore

$$\vec{r} = \vec{r}_L + d\, \hat{k}_L \ , \tag{29}$$

where d is the distance along the beam from the laser source.

Each instance i has a set of random parameters ($k_{i,j}$, $\psi_{i,j}$, and $\phi_{i,j}$), with each parameter having M members, typically on the order of 5 to 20. These parameters generate the full wave spectra

$$S(k_{i,j}, \phi_{i,j}) = S(k_{i,j}) F(\phi_{i,j}) . \tag{30}$$

Each instance also has M angular frequencies $\omega(k_{i,j})$ calculated using Eq. (4) and phase functions

$$\Psi_{i,j}(x, y, t) = \psi_{i,j} + \omega(k_{i,j})t + k_{i,j}[x \cos(\phi_{i,j}) + y \sin(\phi_{i,j})] \tag{31}$$

A given ocean surface instance i has wave components, each with a specific wave number $k_{i,j}$, wave phase $\psi_{i,j}$, and wave direction $\phi_{i,j}$ (allowing only directions where $F(\phi)$ is non-zero) [2], resulting in wave height $\eta_{i,j}$,

$$\eta_{i,j}(x, y, t) = \sqrt{2\, S(k_{i,j}, \phi_{i,j})\, \Delta k_{i,j}\, \Delta\phi_{i,j}}\ \cos\{\Psi_{i,j}(x, y, t)\} . \tag{32}$$

Adding the set of these wave components, spanning the ranges of wave number and direction, provides a good approximation of a sea state, with total wave height

$$\eta_i(x,y,t) = \sum_{j=1}^{M} \sqrt{2\, S(k_{i,j},\phi_{i,j})\, \Delta k_{i,j}\, \Delta\phi_{i,j}}\ \cos\{\Psi_{i,j}(x,y,t)\}\ . \tag{33}$$

Because the wave numbers span many orders of magnitude, obtaining a representative sea state using a reasonable number of components requires reformulation in terms of the logarithm of the wave number,

$$\tilde{k}_j = \ln(k_j)\ , \tag{34}$$

so that

$$\Delta k_j = k_j\, \Delta\tilde{k}_j\ . \tag{35}$$

Using these expressions, Eq. (33) for the wave height becomes

$$\eta_i(x,y,t) = \sum_{l=1}^{M} \sqrt{2\, S(k_{i,j},\phi_{i,j})\, k_{i,j}\, \Delta\tilde{k}_{i,j}\, \Delta\phi_{i,j}}\, \cos\{\Psi_{i,j}(x,y,t)\}. \tag{36}$$

The extents of the wave number and angle, from Eqs. (25) and (27), respectively, yield

$$\Delta\tilde{k}_{i,j}\, \Delta\phi_{i,j} = \frac{L}{M}\pi\ . \tag{37}$$

The total wave height then is

$$\eta_i(x,y,t) = \sqrt{\frac{2\pi L}{M}} \sum_{j=1}^{M} \sqrt{S(k_{i,j},\phi_{i,j})\, k_{i,j}}\ \cos\{\Psi_{i,j}(x,y,t)\}\ . \tag{38}$$

The wave slopes are

$$\frac{d\eta_i(x,y,t)}{dx} = -\sqrt{\frac{2\pi L}{M}} \sum_{j=1}^{M} \sqrt{S(k_{i,j},\phi_{i,j})}\, k_{i,j}^{3/2} \cos(\phi_{i,j})\ \sin\{\Psi_{i,j}(\,x,y,t)\} \tag{39}$$

and

$$\frac{d\eta_i(x,y,t)}{dy} = -\sqrt{\frac{2\pi L}{M}} \sum_{j=1}^{M} \sqrt{S(k_{i,j},\phi_{i,j})}\, k_{i,j}^{3/2} \sin(\phi_{i,j})\ \sin\{\Psi_{i,j}(\,x,y,t)\}\ , \tag{40}$$

resulting in normal $\hat{N}_i$ to the wave

$$\hat{N}_i = \frac{\left(-{}^{d\eta_i}/_{dx}, -{}^{d\eta_i}/_{dy}, 1\right)}{\sqrt{1 + \left({}^{d\eta_i}/_{dx}\right)^2 + \left({}^{d\eta_i}/_{dy}\right)^2}} . \tag{41}$$

The maximum wave height is

$$\eta_{i,max} = \sqrt{\frac{2\pi L}{M}} \sum_{j=1}^{M} \sqrt{S(k_{i,j}, \phi_{i,j})\, k_{i,j}} \;. \tag{42}$$

The maximum slopes are

$$\frac{d\eta_i}{dx}_{max} = -\sqrt{\frac{2\pi\, L}{M}} \sum_{j=1}^{M} \sqrt{S(k_{i,j}, \phi_{i,j})}\, k_{i,j}^{3/2} \cos(\phi_{i,j}) \tag{43}$$

$$\frac{d\eta_i}{dy}_{max} = -\sqrt{\frac{2\pi\, L}{M}} \sum_{j=1}^{M} \sqrt{S(k_{i,j}, \phi_{i,j})}\, k_{i,j}^{3/2} \sin(\phi_{i,j}) \;, \tag{44}$$

resulting in a maximum water surface slope of

$$\dot{\eta}_{i,max} = \sqrt{\left(\frac{d\eta_i}{dx}_{max}\right)^2 + \left(\frac{d\eta_i}{dy}_{max}\right)^2} \;. \tag{45}$$

The intersection of the laser beam with the water surface is the first occurrence when the height of the beam is equal to the height of the water. Setting

$$d_{i,\mathrm{min}} = \frac{\eta_{i,\mathrm{max}} - \vec{r}_{\mathrm{L,z}} + D}{\hat{k}_{\mathrm{L,z}}} \;, \tag{46}$$

step along $d = (d_{i,\mathrm{min}} + l\ D)$ using Eq. (29), where l is an integer starting at zero, until $\vec{r}_z < \eta_i(x, y, t)$. Then iterate to find the location $(x_{i,\mathrm{w}}, y_{i,\mathrm{w}})$ where $\eta_i(x, y, t) = \vec{r}_{\mathrm{z}}(d)$. This yields the intersection location

$$\vec{r}_{i,\mathrm{w}} = \left(x_{i,\mathrm{w}}, y_{i,\mathrm{w}}, \eta_i(x_{i,\mathrm{w}}, y_{i,\mathrm{w}}, t)\right) . \tag{47}$$

Next, check for obscuration by the water surface of the reflected ray to the observer. The direction to the observer is

$$\hat{k}_{i,O} = \frac{\vec{r}_O - \vec{r}_{i,w}}{\left\|\vec{r}_O - \vec{r}_{i,w}\right\|} \;. \tag{48}$$

If the slope of the direction to the observer,

$$\dot{k}_{i,O} = \frac{\hat{k}_{i,O,z}}{\sqrt{\hat{k}_{i,O,x}^2 + \hat{k}_{i,O,y}^2}} \ , \tag{49}$$

is greater than the maximum water surface slope, then no obscuration is possible. If obscuration is possible, step along

$$\vec{r} = \vec{r}_{i,w} + d\ \hat{k}_{i,O} \tag{50}$$

with d a multiple of $D/2$. Obscuration occurs when $\vec{r}_{\mathrm{z}} < \eta_i(x,y,t)$ and the reflected beam does not illuminate the observer. Stepping terminates at this point or when $\vec{r}_{\mathrm{z}} > \eta_{i,\max}$ and there is no longer a possibility of obscuration.

6.0 BRDF

Each instance has a BRDF calculated from the BRDF model. If the reflected beam is obscured, the BRDF is zero for that instance. If there is no obscuration, the BRDF is calculated from models of either a whitecap or a smooth water surface. The presence of a whitecap determines which model is relevant. These models are detailed in the following two sections.

6.1 Whitecap Presence and BRDF

In general, the fraction of whitecaps over a large extent of water increases with wind speed, and there are several empirical models for this fraction. Wu [10] gives the fraction F_{WC} as

$$F_{\mathrm{WC}} = \min(1.0, 1.7 \times 10^{-6} \cdot W_{10}^{3.75}) \ , \tag{51}$$

where W_{10} has units of (m/s). The whitecap fraction increases until the wind speed is approximately 35 m/s (hurricane force), at which point the water surface is entirely covered in whitecaps.

Each instance of the probabilistic water BRDF model calculates a specific intersection of the laser beam with the water surface. Therefore, a fraction of whitecaps is not appropriate for this model. Instead, an acceleration criteria proposed by Chen [11] determines if a whitecap is present at the location of intersection. Whitecaps occur at or near the crest of a wave, when the vertical acceleration is less than –0.39 g. Using the wave height given by Eq. (38), the vertical acceleration of a wave is

$$\frac{d^2\eta_i(x,y,t)}{dt^2} = \ddot{\eta}_i = -\sqrt{\frac{2\pi L}{M}} \sum_{j=1}^{M} \omega^2(k_{i,j}) \sqrt{S(k_{i,j},\phi_{i,j})\, k_{i,j}}\ \cos\{\Psi_{i,j}(x,y,t)\} \ . \tag{52}$$

Simulations of whitecap formation as a function of wind speed using Eq. (52) yielded lower fractions than those given by Eq. (51). Therefore, the whitecap model includes the additional feature of feathering, or blending, the whitecap with the surrounding smooth water surface. Chen [11] presents an involved method for feathering. A more tractable model, inspired by that of Chen, is the probability of a whitecap P_{WC}, given by

$$P_{\mathrm{WC}} = \begin{cases} 1 & \ddot{\eta}_i \le -0.39\,g \\ \dfrac{\ddot{\eta}_i + \alpha g}{g(\alpha - 0.39)} & -0.39\,g < \ddot{\eta}_i \le -\alpha\,g \\ 0 & -\alpha\,g < \ddot{\eta}_i \end{cases} . \quad (53)$$

The value of α depends on the wind speed and was determined from simulations of the fraction of whitecaps as a function of α for fixed wind speeds. Linear fits of the fraction as a function of wind speed determined the value of α at which the fit equals the fraction given by Eq. (51) for that wind speed, yielding

$$\alpha = -0.0022\,w^* + 0.4448\,, \quad (54)$$

where w^* has units of cm/s. The whitecap fractions from Eq. (51) and simulations using Eqs. (53) and (54) are shown in Fig. 3.

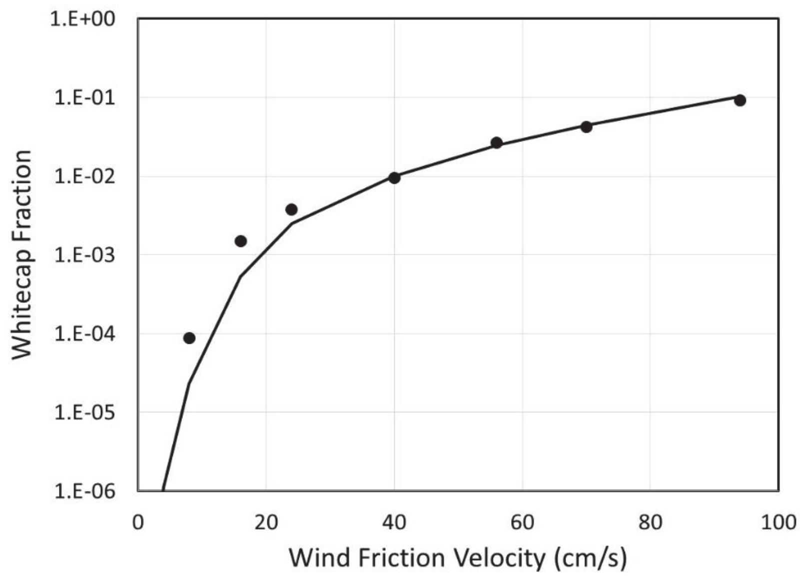

Figure 3. Whitecap fraction calculated from Eq. (51) – solid line – and simulations using Eqs. (52) to (54) – circles

If a whitecap is present at the location of intersection of the laser beam with the water surface, the BRDF $f_{r,\mathrm{WC}}$ is Lambertian and given by

$$f_{r,\mathrm{WC}} = \frac{1}{\pi}[0.22\,\exp\{-1.75(\max(\lambda, 0.6) - 0.6)\}]\,, \quad (55)$$

where λ is the wavelength in microns [12,13,14].

6.2 Smooth Water BRDF

If a whitecap is not present, then the BRDF for smooth water is appropriate for that instance. The smooth water BRDF is a faceted model, similar to the Maxwell-Beard BRDF model for materials [15]. The surface is composed of facets smaller than the beam diameter, with a distribution of normals peaked about the global normal. Reflections from the laser source to an observer are specular reflections from correctly aligned facets. The smooth water BRDF $f_{r,\mathrm{SW}}$ is

$$f_{r,sw} = \frac{\pi}{4} \frac{1}{\cos\theta_i \ \cos\theta_r \ \cos^4\xi} \rho_{SW}(\zeta)\, p(\xi)\, G(\theta_i, \theta_r), \tag{56}$$

where the angles are illustrated in Fig. 4, ρ_{SW} is the water specular reflectance, p is the wave slope probability function, and G is the shadowing function [16]. The geometry of smooth water BRDF for a wave instance is shown in Fig. 4. The wave normal is $\hat{N}_i$, which usually does not align with the global vertical $\hat{N}$, $\hat{H}$ is the half-angle between the incident and reflected directions, and the other angles are indicated.

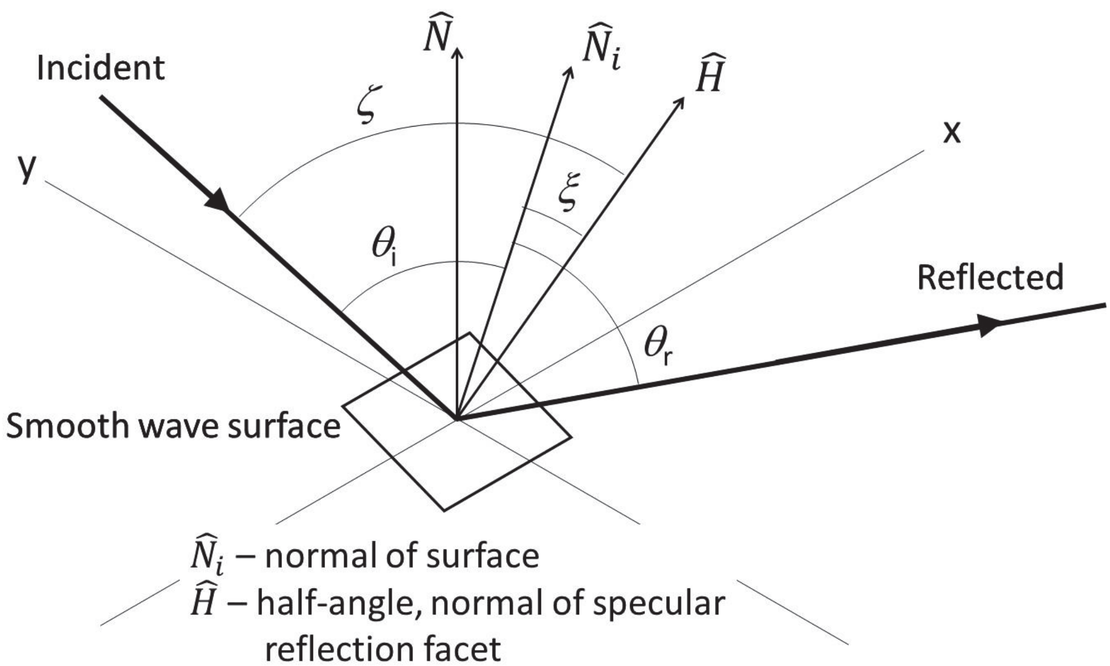

Figure 4. Directions and angles for smooth water BRDF

For laser and observer locations $\vec{r}_{\mathrm{L}}$ and $\vec{r}_{\mathrm{O}}$, respectively, and laser beam-water intersection location $\vec{r}_{i,\mathrm{w}}$ for instance i, from Eq. (47), the incident and reflected direction vectors are

$$\hat{V}_{\mathrm{s}} = \frac{\vec{r}_{\mathrm{L}} - \vec{r}_{i,\mathrm{w}}}{\left\|\vec{r}_{\mathrm{L}} - \vec{r}_{i,\mathrm{w}}\right\|} \quad \text{and} \tag{57}$$

$$\hat{V}_{\mathrm{r}} = \frac{\vec{r}_{\mathrm{O}} - \vec{r}_{i,\mathrm{w}}}{\left\|\vec{r}_{\mathrm{O}} - \vec{r}_{i,\mathrm{w}}\right\|} \quad . \tag{58}$$

Note that the subscript i for wave instance is implicit in this section to avoid confusion with the angle of incidence θ_i.

The half-angle vector $\hat{H}$ of the wave facet reflecting light from the laser to the observer is

$$\hat{H} = \frac{\hat{V}_\mathrm{s} + \hat{V}_\mathrm{r}}{\left\|\hat{V}_\mathrm{s} + \hat{V}_\mathrm{r}\right\|} \quad . \tag{59}$$

Since the smooth water BRDF uses a facet model, $\hat{H}$ is also the normal of the facet specularly reflecting the laser beam.

The angles of incidence and reflectance relative to the wave surface normal are

$$\cos\theta_i = \hat{V}_s \cdot \hat{N}_i \quad \text{and} \quad \cos\theta_r = \hat{V}_r \cdot \hat{N}_i \ . \tag{60}$$

The angle of incidence relative to the facet normal is

$$\cos\zeta = \hat{V}_\mathrm{s} \cdot \hat{H} = \hat{V}_\mathrm{r} \cdot \hat{H} \ . \tag{61}$$

The normal-incidence reflectance ρ_n of the water surface is

$$\rho_\mathrm{n} = \left(\frac{n-1}{n+1}\right)^2 , \tag{62}$$

where n is the index of refraction. The index is known at wavelengths from 200 nm to 200 µm as a function of salinity [17, 18], and is approximately 1.33 at 1 µm, resulting in $\rho_\mathrm{n} = 0.020$. The water reflectance for unpolarized light is approximated by [19]

$$\rho_{SW}(\zeta) = \rho_\mathrm{n} + (1-\rho_\mathrm{n})(1-\cos\zeta)^5 \, . \tag{63}$$

The Nakajima-Tanaka shadowing function $G(\theta_i, \theta_r)$ is

$$\sigma^2 = 5.34 \times 10^{-3}\, W_{10} \ , \tag{64}$$

$$\nu_i = \frac{\cos\theta_i}{\sigma\sqrt{1-\cos\theta_i}} \quad \text{and} \quad \nu_r = \frac{\cos\theta_r}{\sigma\sqrt{1-\cos\theta_r}} \ , \tag{65}$$

$$F(\nu) = \frac{1}{2}\left[\frac{\exp(-\nu^2)}{\sqrt{\pi}\,\nu^2} - \mathrm{erfc}(\nu)\right] , \qquad \text{and} \tag{66}$$

$$G = \frac{1}{1 + F(\nu_i) + F(\nu_r)} \ . \tag{67}$$

Here, the units of W_{10} are (m/s) and the maximum value of G is 1.

The wave slope probability function has two factors, the Gaussian first-order term p_0 and the correction for kurtosis and skewness p_{ks}. The wave slope probability function also depends on the wind direction, with upwind and crosswind horizontal direction unit vectors $\widehat{W}_u$ and $\widehat{W}_c$, respectively. If the wind direction is at an angle ϕ_W with the local x-axis, then

$$\widehat{W}_u = (\cos\phi_W, \sin\phi_W, 0) \text{ and } \widehat{W}_c = (-\sin\phi_W, \cos\phi_W, 0) \ . \tag{68}$$

The upwind and crosswind half-angles are

$$\widehat{H}_u = \frac{\widehat{H} - (\widehat{H}\cdot\widehat{W}_c)\widehat{W}_c}{|\widehat{H} - (\widehat{H}\cdot\widehat{W}_c)\widehat{W}_c|} \text{ and } \widehat{H}_c = \frac{\widehat{H} - (\widehat{H}\cdot\widehat{W}_u)\widehat{W}_u}{|\widehat{H} - (\widehat{H}\cdot\widehat{W}_u)\widehat{W}_u|} \ , \tag{69}$$

with corresponding normals

$$\widehat{N}_u = \frac{\widehat{N} - (\widehat{N}\cdot\widehat{W}_c)\widehat{W}_c}{|\widehat{N} - (\widehat{N}\cdot\widehat{W}_c)\widehat{W}_c|} \text{ and } \widehat{N}_c = \frac{\widehat{N} - (\widehat{N}\cdot\widehat{W}_u)\widehat{W}_u}{|\widehat{N} - (\widehat{N}\cdot\widehat{W}_u)\widehat{W}_u|} \ . \tag{70}$$

The wave normal variances are

$$\cos\xi_u = \widehat{H}_u\cdot\widehat{N}_u \ , \qquad \cos\xi_c = \widehat{H}_c\cdot\widehat{N}_c \ , \qquad \text{and} \qquad \cos\xi = \widehat{H}\cdot\widehat{N}_i \ . \tag{71}$$

The Gaussian first-order term is

$$p_0 = \frac{1}{2\pi\,\sigma_u\,\sigma_c}\exp\left\{-\frac{1}{2}\left(\frac{{\xi_u}^2}{{\sigma_u}^2} + \frac{{\xi_c}^2}{{\sigma_c}^2}\right)\right\} = \frac{1}{2\pi\,\sigma_u\,\sigma_c}\exp\left\{-\frac{1}{2}\left(U^2 + C^2\right)\right\} , \tag{72}$$

with

$$U = \frac{\xi_u}{\sigma_u} \quad \text{and} \quad C = \frac{\xi_c}{\sigma_c} \ . \tag{73}$$

The variances [4] are

$$\sigma_u^2 = M_u\left[\begin{array}{l}\left\{1 - \exp\left(-\frac{W_{10}}{36.8188}\right)\right\}\mathrm{erfc}\left\{\left(\frac{1}{D}\frac{1}{(1.3261\,W_{10} + 6.2780)}\right)^{(0.0033\,W_{10}+0.2666)}\right\} \\ +\exp\left(-\frac{W_{10}}{36.8188}\right)\mathrm{erfc}\left\{\left(\frac{1}{D}\frac{1}{(7.0628\,W_{10} + 24.2598)}\right)^{(0.0240\,W_{10}+0.4956)}\right\}\end{array}\right] \tag{74}$$

and

$$\sigma_c^2 = M_c\left[\begin{array}{l}\left\{1 - \exp\left(-\frac{W_{10}}{35.1072}\right)\right\}\mathrm{erfc}\left\{\left(\frac{1}{D}\frac{1}{(1.2156\,W_{10} + 11.3065)}\right)^{(0.0021\,W_{10}+0.2965)}\right\} \\ +\exp\left(-\frac{W_{10}}{35.1072}\right)\mathrm{erfc}\left\{\left(\frac{1}{D}\frac{1}{(7.0596\,W_{10} + 24.4595)}\right)^{(0.0241\,W_{10}+0.5021)}\right\}\end{array}\right] \tag{75}$$

with $1/e^2$ beam diameter D (m), wind speed W_{10} (m/s), and large spot limits M for variances

$$M_\mathrm{u} = 0.00316\, W_{12.5} \text{ and} \tag{76}$$

$$M_\mathrm{c} = (0.003 + 0.00192\, W_{12.5})\,. \tag{77}$$

The correction for kurtosis and skewness is

$$\begin{aligned} \mathrm{p_{ks}} = 1 - \frac{1}{2}\mathrm{c}_{21}(C^2 - 1) - \frac{1}{6}\mathrm{c}_{03}(U^3 - 3U) + \frac{1}{24}\mathrm{c}_{40}(C^4 - 6C^2 + 3) \\ + \frac{1}{4}\mathrm{c}_{22}(C^2 - 1)(U^2 - 1) + \frac{1}{24}\mathrm{c}_{04}(U^4 - 6U^2 + 3) \end{aligned} \tag{78}$$

where $c_{21} = 0.01 - 0.0086\, W_{12.5}$, $c_{03} = 0.04 - 0.033\, W_{12.5}$, $c_{40} = 0.40$, $c_{22} = 0.12$, and $c_{04} = 0.23$ [1]. The wave slope probability function is

$$p(\xi) = p_0 \cdot p_\mathrm{ks}\,. \tag{79}$$

7.0 CALCULATION SUMMARY

The following steps are required to implement the probabilistic water BRDF model for engagement scenarios involving reflections of laser beams from water surfaces. An engagement scenario consists of laser and observer locations at discrete times, and the laser aim point or direction at these times.

First, set the static parameters for the engagement scenario. These are the wind speed and direction (typically a wind friction velocity or a speed at a given height above the mean surface with direction aligned to a global axis), the water depth if close to shore, and the number of wave numbers M for each instance and the number of instances N. While the beam diameter may vary with time, the effect of this variation is slight so fix the beam diameter to a representative or minimum value. Calculate the wind speeds using the equations in Section 3.

Next, for each instance, draw random values for the wave numbers, phase angles, and angles, and calculate the wave energy spectra using the equations in Section 4. These wave energy spectra apply to all locations and times of the engagement scenario.

Finally, at each time and observer location, calculate the intersection location of the laser beam with the water surface and the normal of the water surface at this location for each instance using the equations in Section 5. Use this location and normal to calculate the BRDF using the equations in Section 6. Accumulate the BRDFs at each time and observer location over all instances, and then calculate the statistics of the BRDF. These statistics are typically the mean and standard deviation. These statistics are the probabilistic water BRDF for that time and observer location.

8.0 EXAMPLE RESULTS

The probabilistic water BRDF model obviously has many inputs, so generalizing the model is not possible. However, illustrating some general trends with examples is feasible. This section uses a base engagement scenario with variations. The base scenario has a wind friction velocity w^* = 8 cm/s (light breeze), wind direction $\phi_W = 0°$ (along the x-axis), laser beam diameter D = 15 cm, angle of incidence $\theta_i = 30°$, and angle with the wind direction $\phi_i = 0°$. The number of wave numbers M = 5 and the number of instances N = 50.

An example of the wave heights resulting from this base scenario are shown in Fig. 5 both as a function of distance for selected times, and as a function of time at a fixed location. The waves are semi-periodic with distance and time, as expected.

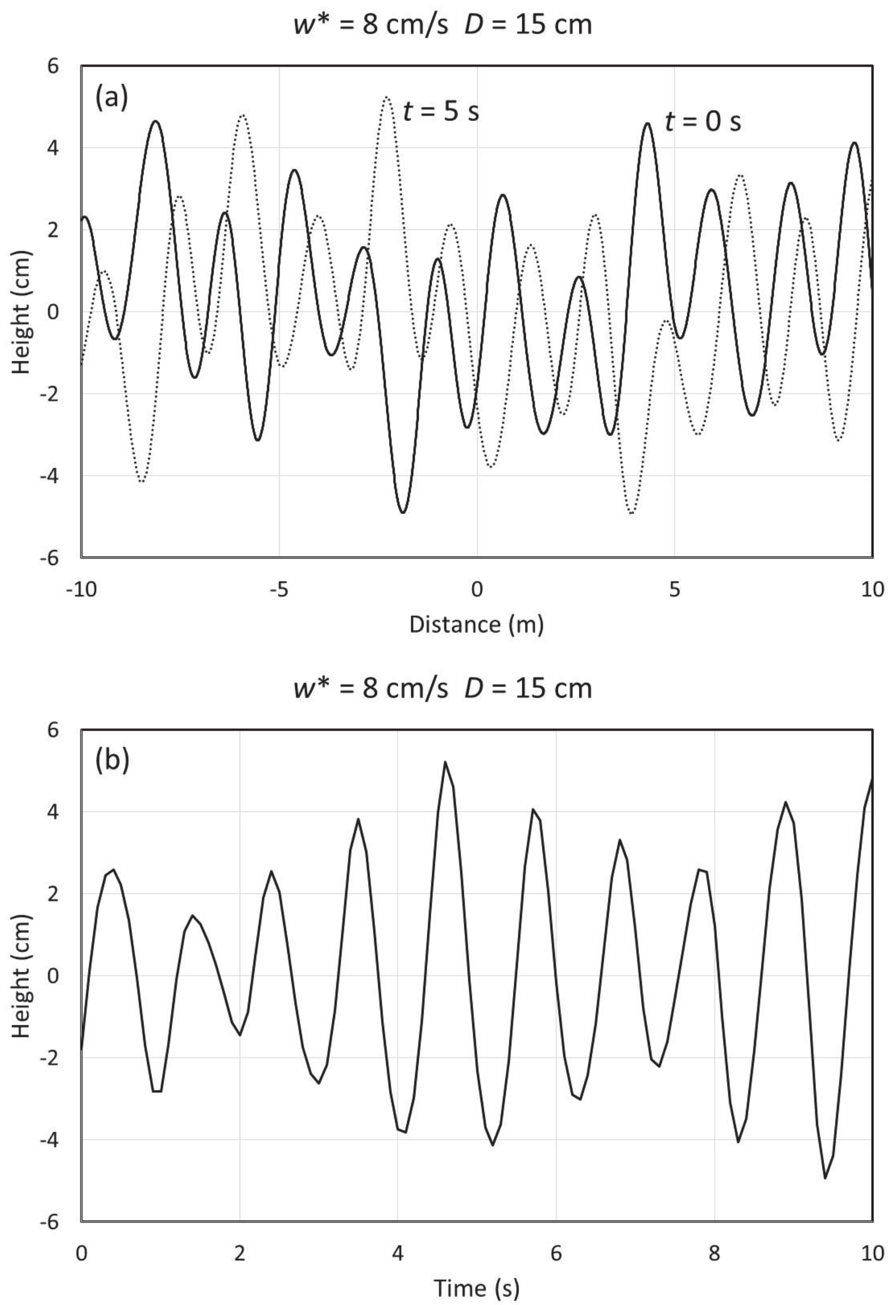

Figure 5. Illustrative wave height (a) as a function of distance at indidated times and (b) as a function of time for the base engagement scenario.

In general, the water BRDF has a maximum in the specular reflection direction with a Gaussian distribution around this maximum. This distribution has both in-plane and out-of-plane components. Therefore, using these two components to illustrate the water BRDF is convenient. This concept of in-plane and out-of-plane is also applicable to the empirical water BRDF detailed in Section 9.

In-plane refers to the plane of incidence, defined by the global normal direction (vertical) and the direction of incidence or reflection. In general, this is the *x*-*z* plane if the engagement scenario aligns the laser and aim point in this plane. Out-of-plane refers to the plane perpendicular to the plane of incidence and containing the direction of reflection. It is therefore perpendicular to the *x*-*z* plane and at an angle θ_i to the vertical.

With the *x*-*z* plane as in-plane, and θ_i the angle of incidence, θ_r the in-plane angle of reflection, and ϕ_r the out-of-plane angle of reflection, the incident direction is

$$\hat{k}_i = (-\sin\theta_i\,, 0, \cos\theta_i)\ , \tag{80}$$

the in-plane reflected direction is

$$\hat{k}_r = (\sin\theta_r\,, 0, \cos\theta_r)\ , \tag{81}$$

and the out-of-plane reflected direction is

$$\hat{k}_r = (\sin\theta_i\cos\phi_r\,, \cos\theta_i\sin\phi_r\,, \cos\theta_i\cos\phi_r)\ . \tag{82}$$

The in-plane and out-of-plane BRDF for each instance of the base engagement scenario are shown in Figs. 6, and the average BRDFs are shown in Fig. 7. Also shown in Fig. 7 is the flat wave BRDF, the BRDF assuming no wave geometry. The instances of BRDF span a significant range in both angle of reflection and magnitude. These ranges result from variations in the wave normal at the location of intersection with the laser beam. In-plane variations account for the increase in the magnitude of BRDF in Fig. 6(a) as the angle of reflection increases. This increase in angle results in smaller cosine terms in the denominator or Eq. (56) and greater specular reflectance in Eq. (63). Out-of-plane variations account for the range in angle of the maximum BRDF in Fig. 6(b) and for the decrease in magnitude in both Figs. 6(a) and 6(b).

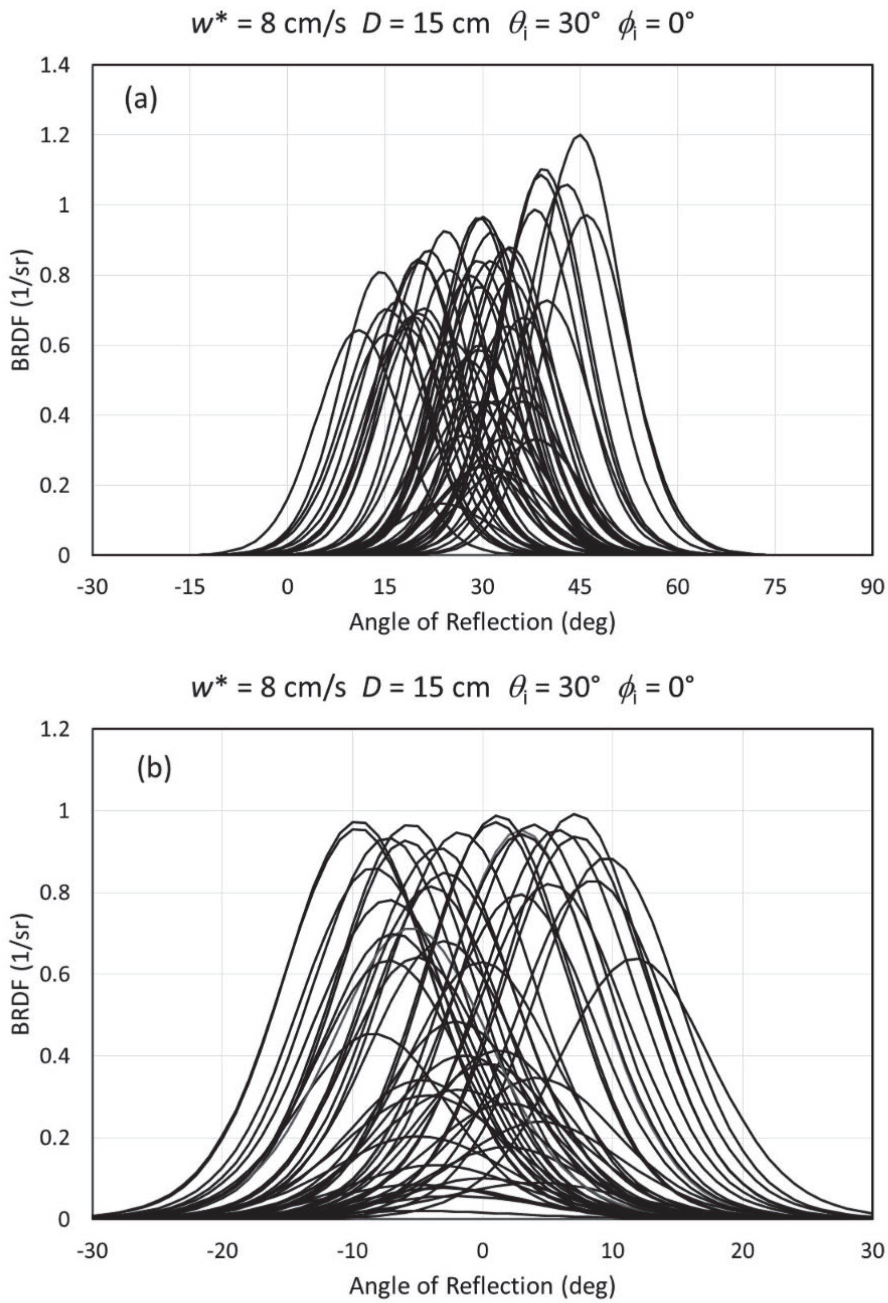

Figure 6. All instances of the (a) in-plane and (b) out-of-plane BRDF for the base engagement scenario.

Both the in-plane and out-of-plane average BRDFs in Fig. 7 are well behaved, with maximums at, or close to, the specular reflection angle. The maximum of the average is less than that of the flat wave BRDF, while the width is greater, as expected from the instances shown in Fig. 6.

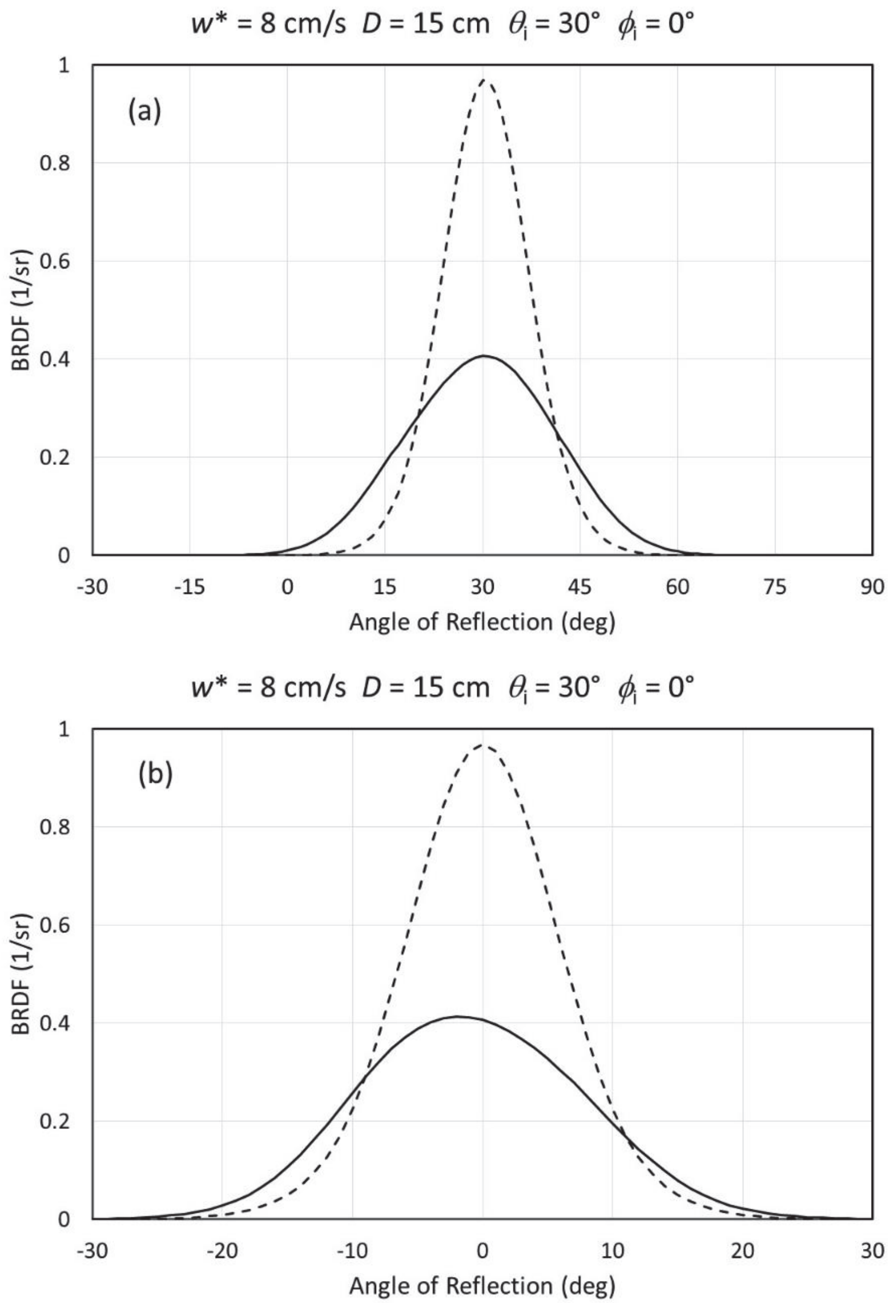

Figure 7. Average of the BRDF instances (solid line) and flat wave BRDF (dashed line) of the (a) in-plane and (b) out-of-plane instances of the base engagement scenario.

The variation with wind friction velocity is shown in Fig. 8. The maximum BRDF decreases rapidly with increasing wind velocity. This decrease is inversely proportional to the wind friction speed and is greater than an order of magnitude over the range.

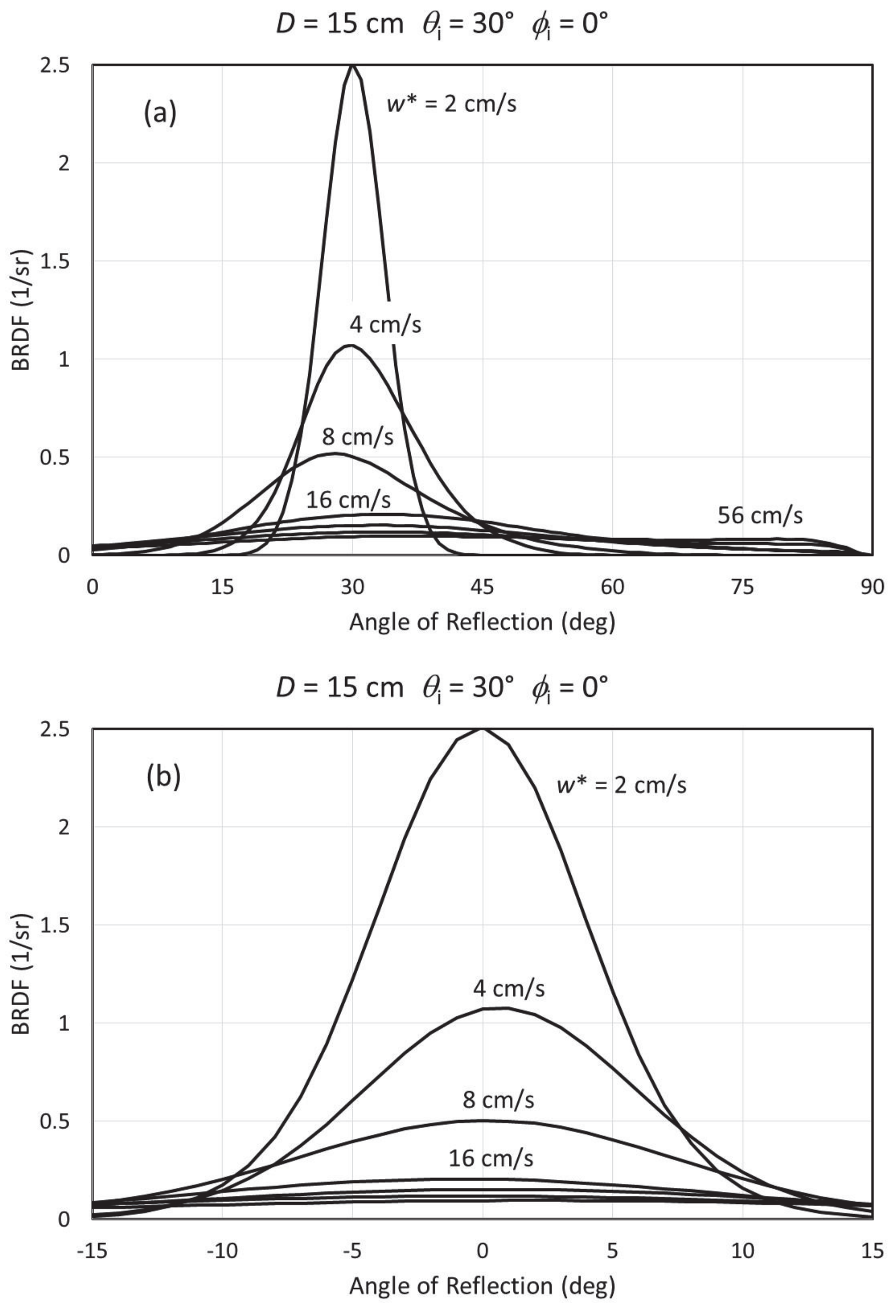

Figure 8. Average (a) in-plane and (b) out-of-plane BRDF for the base engagement scenario with the indicated wind friction velocities.

An aspect of water BRDF not usually present in faceted BRDF models is shown in Fig. 9. A "secondary" BRDF peak occurs at angles of reflection near 80°. This is due to large wave normal variances in Eq. (72) and small cosine terms in the denominator of Eq. (56). Increasing wind friction velocity and angle of incidence makes these "secondary" peaks more pronounced.

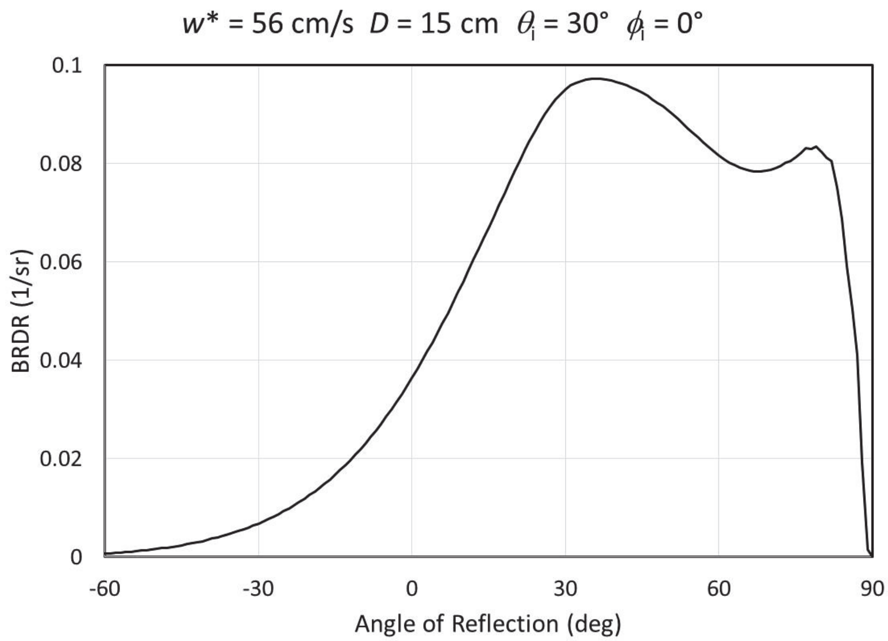

Figure 9. Average BRDF for the base engagement scenario at the maximum wind friction velocity.

The variation with laser beam diameter is shown in Fig. 10. There are no definite trends with beam diameter, other than a possible slight increase in maximum BRDF with increasing beam diameter.

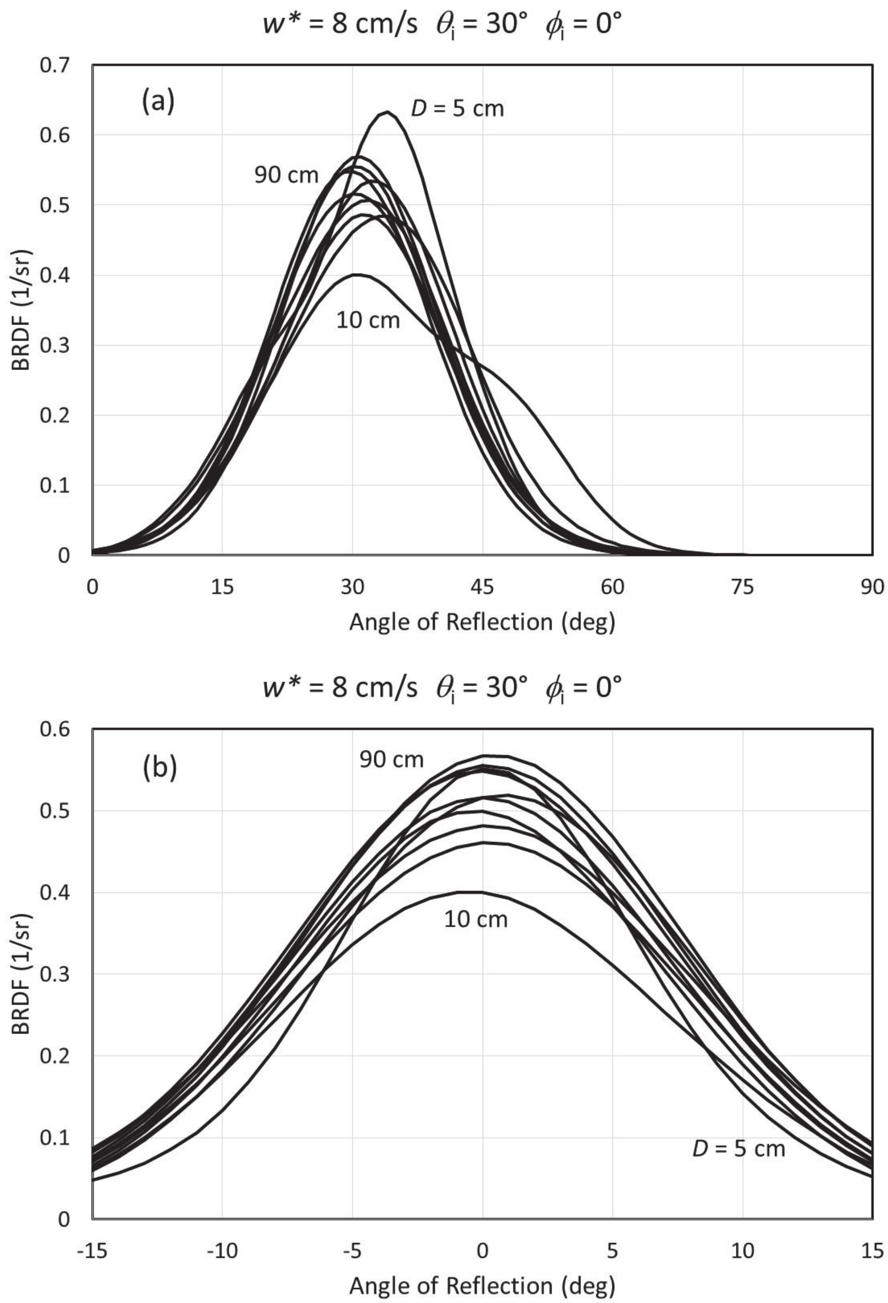

Figure 10. Average (a) in-plane and (b) out-of-plane BRDF for the base engagement scenario with the indicated laser beam diameters at 5 cm increments.

The variation with angle of incidence is shown in Fig. 11. As expected from Eqs. (56) and (63), the maximum BRDF increases with increasing angle of incidence, with the increase being particularly steep at large angles of incidence.

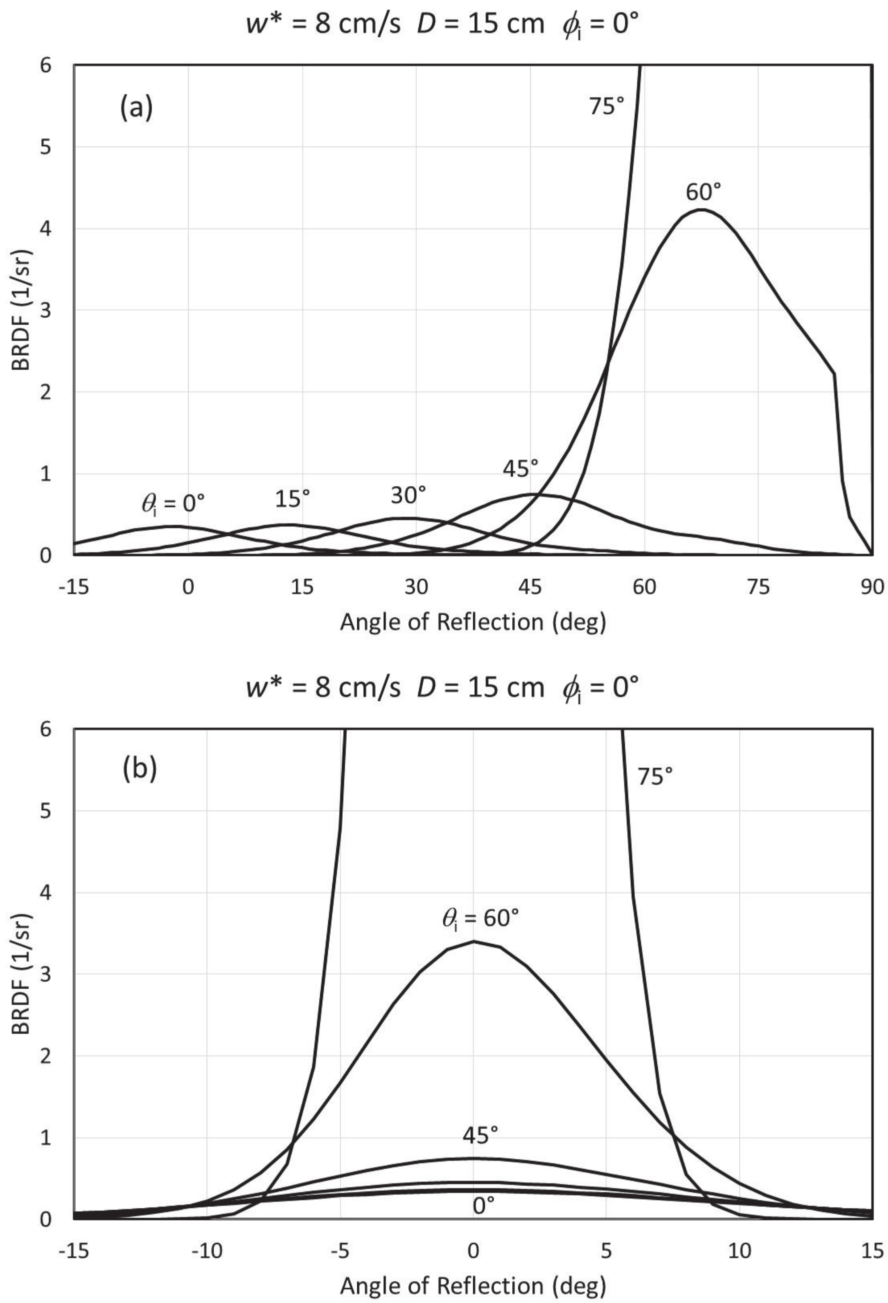

Figure 11. Average (a) in-plane and (b) out-of-plane BRDF for the base engagement scenario with the indicated angles of incidence.

Finally, the dependence on angle with respect to the wind direction is shown in Fig. 12. Dependence of the in-plane BRDF is slight, while the out-of-plane BRDF shifts slightly with increasing angle.

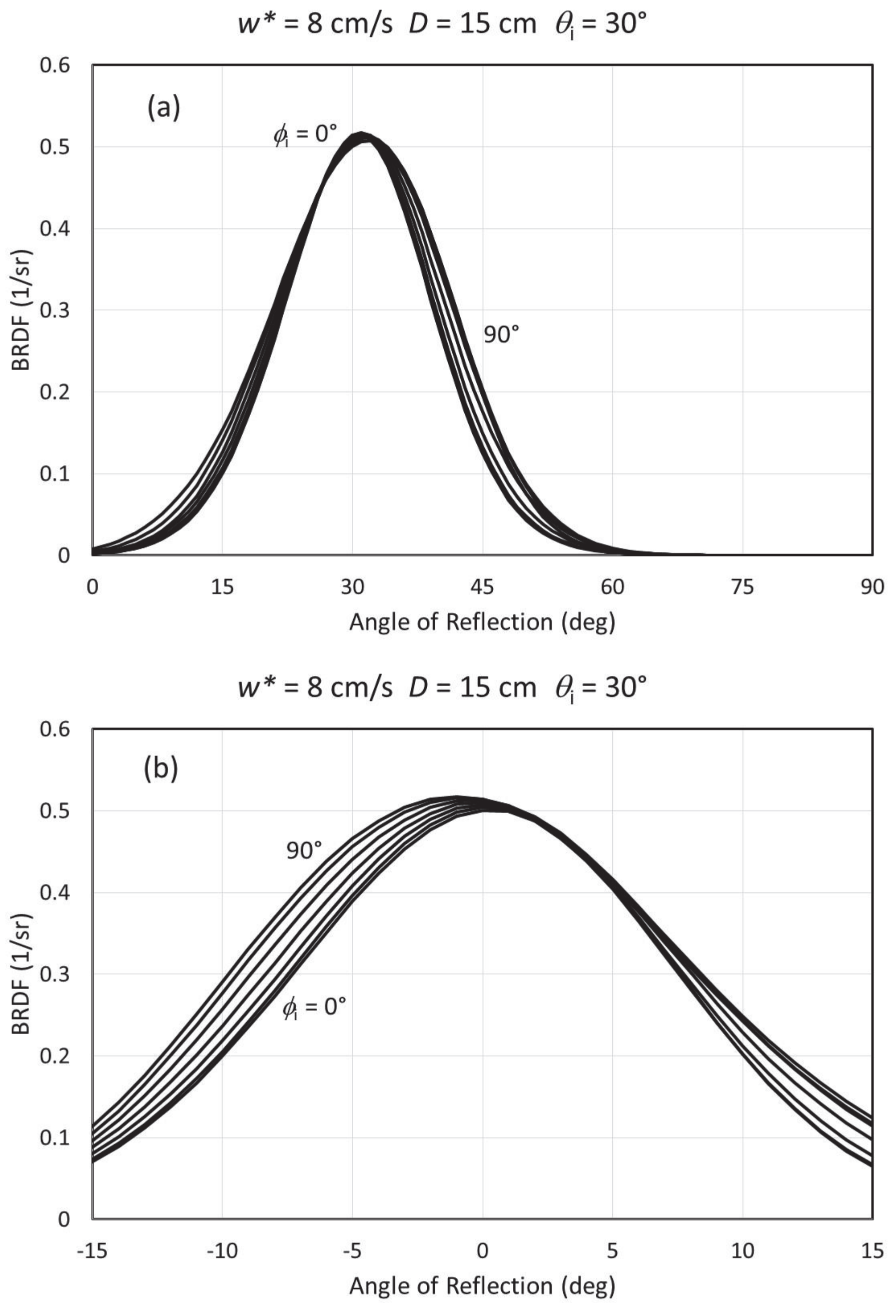

Figure 12. Average (a) in-plane and (b) out-of-plane BRDF for the base engagement scenario with the indicated angles relative to the wind direction in 15° increments.

9.0 EMPIRICAL WATER BRDF MODEL

An empirical water BRDF model provides an alternative to employing the full probabilistic water BRDF model detailed in previous sections, with a corresponding decrease in computational time. It also offers a set of stable BRDF values, without the variations that occur when re-computing a probabilistic value.

The empirical water BRDF model has in-plane and out-of-plane components, as introduced in Section 8. The laser, water intersection, and observer locations are $\vec{r}_L$, $\vec{r}_W$, and $\vec{r}_O$, respectively. The water surface has normal $\hat{n} = (0,0,1)$. The incident direction $\hat{k}_i$ is

$$\hat{k}_i = \frac{\vec{r}_L - \vec{r}_W}{|\vec{r}_L - \vec{r}_W|}\ , \tag{83}$$

and the specular reflection direction is

$$\hat{k}_r = 2\big(\hat{n} \cdot \hat{k}_i\big)\hat{n} - \hat{k}_i\ . \tag{84}$$

The in-plane and out-of-plane normals are

$$\hat{n}_{\text{in}} = \frac{\hat{n} \times \hat{k}_r}{\big|\hat{n} \times \hat{k}_r\big|} \quad \text{and} \quad \hat{n}_{\text{out}} = \hat{k}_r \times \hat{n}_{\text{in}}\ . \tag{85}$$

The direction to the observer is

$$\hat{k}_O = \frac{\vec{r}_O - \vec{r}_W}{|\vec{r}_O - \vec{r}_W|}\ , \tag{86}$$

The components of this direction in the two planes are

$$\hat{k}_{O,\text{in}} = \frac{\hat{k}_O - \big(\hat{k}_O \cdot \hat{n}_{\text{in}}\big)\hat{n}_{\text{in}}}{\big|\hat{k}_O - \big(\hat{k}_O \cdot \hat{n}_{\text{in}}\big)\hat{n}_{\text{in}}\big|} \ \text{and}\ \hat{k}_{O,\text{out}} = \frac{\hat{k}_O - \big(\hat{k}_O \cdot \hat{n}_{\text{out}}\big)\hat{n}_{\text{out}}}{\big|\hat{k}_O - \big(\hat{k}_O \cdot \hat{n}_{\text{out}}\big)\hat{n}_{\text{out}}\big|}\ . \tag{87}$$

The angles between the direction to the observer and the specular direction in the two planes (θ_{r} for in-plane and ϕ_{r} for out-of-plane) are

$$\cos\theta_{\mathrm{r}} = (0,0,1) \cdot \hat{k}_{O,\text{in}} \quad \text{and} \quad \cos\phi_{\mathrm{r}} = \hat{k}_r \cdot \hat{k}_{O,\text{out}}\ . \tag{88}$$

The probabilistic water BRDF model generates results as a function of wind friction velocity, laser beam diameter, and angle of incidence. The average in-plane BRDF is $f_r(\theta_r)$ with standard deviation $u_{f_r}(\theta_r)$; the average out-of-plane BRDF width is $\sigma(0)$ with standard deviation $u_\sigma(0)$; and the average out-of-plane peak offset is $\delta(\theta_i)$ with standard deviation $u_\delta(\theta_i)$. For an observer location,

$$\sigma = \begin{cases} \sigma(0)\cos\left(\dfrac{\theta_i + \theta_r}{2}\right) & \theta_r < \theta_i \\ \sigma(0)\cos(\theta_i) & \theta_r \geq \theta_i \end{cases}\ , \tag{89}$$

with BRDF at this location of

$$f_r(\vec{r}_O) = f_r(\theta_r)\exp\left[-\left(\frac{\phi_r - \delta}{\sigma}\right)^2\right]. \tag{90}$$

Typically, $\delta = 0$ in Eq. (90). The in-plane BRDF and out-of-plane width and peak offset values and standard uncertainties provide the basis for Monte Carlo simulations. Alternatively, the uncertainty in the BRDF at the observer location is

$$\left[\frac{u(f_r)}{f_r}\right]^2 = \left[\frac{u_{f_r}(\theta_r)}{f_r(\theta_r)}\right]^2 + \left[2\left(\frac{\phi_r}{\sigma}\right)^2 \frac{u_\sigma(0)}{\sigma(0)}\right]^2 + \left[2\left(\frac{\phi_r}{\sigma}\right)^2 \frac{u_\delta(\theta_i)}{\phi_r}\right]^2 . \quad (91)$$

10.0 CONCLUSIONS

Reflections of incident laser beams by water are a potential concern. Surface waves complicate the BRDF of water, as they depend on the prevailing wind speed and direction and introduce a probabilistic aspect into modeling the BRDF of water. The model of water BRDF presented here accounts for waves over many length scales. A probabilistic wave energy spectra models those with wavelengths longer than the diameter of the incident laser beam to yield a water surface normal at the location of incidence. This normal changes with location and time according to the wave energy spectra. Facets with a slope distribution function model the shorter wavelengths. The BRDF depends primarily on the wind speed and locations of the laser, intersection of the laser beam with the water surface, and observer. Examples of BRDF as a function of wind speed and angles show that the BRDF is significant only close to the specular direction and for small wind speeds. An empirical model for more rapid calculations has in-plane and out-of-plane components with values based upon results from the probabilistic model.

11.0 REFERENCES

1. Cox, C., Munk, W., "Measurement of the Roughness of the Sea Surface from Photographs of the Sun's Glitter," *J. Opt. Soc. Am.* **44**, 1954, pp. 838-850.

2. Pierson, W. J., "The Theory and Applications of Ocean Wave Measuring Systems at or Below the Sea Surface, on Land, from Aircraft, and from Spacecraft," NASA Report CR-2646, January 1976.

3. Bailey, A.W., Early, E.A., Ahmed, E., and Kumru, S.S., "Probabilistic Water Bidirectional Reflectance Distribution Function," Air Force Research Laboratory Report AFRL-RH-FS-TR-2021-0006, June 2021.

4. Bailey, A.W., Early, E.A., Kumru, S., "A Water Reflection BRDF Model for Use in the HELCAT Code," Air Force Research Laboratory Report AFRL-RH-FS-TR-2019-0017, September 2019.

5. Aguirre, D., Gay, S., Jaeger, N., Kelly, P., Shriver, P., Davis, J., "Ocean Glint Analysis Methodology," Satellite Assessment Center, AFRL/RDTE, March 2010.

6. Cardone, V.J., "Specification of the Wind Distribution in the Marine Boundary Layer for Wave Forecasting," New York University School of Engineering and Science Geophysical

Sciences Laboratory Technical Report TR69-1, prepared for the U. S. Naval Oceanographic Office, December 1969.

7. National Weather Service, https://www.weather.gov/mfl/beaufort, Accessed 1 June 2021.

8. Bjerkaas, A.W., Riedel, F.W., "Proposed Model for Elevation Spectrum of a Wind-Roughened Sea Surface," John Hopkins University Applied Physics Laboratory Technical Memorandum TG 1328, December 1979.

9. Hasselmann, K., et al., "Measurements of Wind-Wave Growth and Swell Decay during the Joint North Sea Wave Project (JONSWAP),", *Ergnzungsheft Zer Deutschen Hydrographischen Zeitschrift Reihe* **A8**, 1973.

10. Wu, J., "Variations of Whitecap Coverage with Wind Stress and Water Temperature," *J. Phys. Oceanography* **18**, 1988, pp. 1448-1454.

11. Chen, L., Jin, Y., Yin, Y., "Ocean Wave Rendering with Whitecap in the Visual System of a Maritime Simulator," *Journal of Computing and Information Technology* **25**, 2017, pp. 63-76.

12. Koepke, P., "Effective reflectance of oceanic whitecaps," *Applied Optics* **23**, 1984, pp. 1816-1824.

13. Frouin, R. J., Deschamps, P.-Y., "AVRIS measurements of spectral reflectance characteristics of whitecaps," Proc. SPIE 4154, Hyperspectral Remote Sensing of the Ocean, January 2001.

14. Schwenger, F., Repasi, E., "Simulation of oceanic whitecaps and their reflectance characteristics in the short wavelength infrared," *Applied Optics* **56**, 2017, pp. 1662-1673.

15. Maxwell, J.R. and Beard, J., "Bidirectional Reflectance Model Validation and Utilization," ERIM Technical Report AFAL-TR-73-303, 1973.

16. Ross, V., Dion, D., Potvin, G., "Detailed analytical approach to the Gaussian surface bidirectional reflectance distribution function specular component to the sea surface," *J. Opt. Soc. Am.* **22**, 2005. pp. 2442-2453.

17. Hale, G.M., Querry, M.R., "Optical Constants of Water in the 200-nm to 200-µm Wavelength Region," *Applied Optics* **12**, 1973, pp. 555-563.

18. Friedman, D., "Infrared Characteristics of Ocean Water (1.5-14 µ)," *Applied Optics* **8**, 1969, pp. 2073-2078.

19. Schlick, C., "An Inexpensive BRDF Model for Physically-Based Rendering," Computer Graphics Forum **13**, 1994, pp. 233-246.